Available online at www.sciencedirect.com
ScienceDirect
Atmospheric Environment 40 (2006) 7770–7785
ATMOSPHERIC ENVIRONMENT
www.elsevier.com/locate/atmosenv

Testing kernel density reconstruction for Lagrangian photochemical modelling

Fabio Monforti[a,*], Lina Vitali[a], Gianni Pagnini[a], Rita Lorenzini[a], Luca Delle Monache[b], Gabriele Zanini[a]

[a]*ENEA PROT-INN, FUS-MAG and CAMO sections, via Martiri di Monte Sole 4, I-40129 Bologna, Italy*
[b]*Lawrence Livermore National Laboratory, 7000 East Avenue, L-103 Livermore, CA 94551, USA*

Received 1 February 2006; received in revised form 26 July 2006; accepted 26 July 2006

Abstract

In recent years, a number of pioneering works have shown as Lagrangian models can be of great interest when dealing with photochemistry, provided that special care is given in the reconstruction of chemicals concentration in the atmosphere. Density reconstruction can be performed through the so-called "box counting" method: an Eulerian grid for chemistry is introduced and density is computed counting particles in each box. In this way one of the main advantages of the Lagrangian approach, the grid independence, is lost. In this paper, a new approach to Lagrangian photochemical modelling is investigated and the chemical module of the Photochemical Lagrangian Particle Model (PLPM) is described and fully tested for stability, reliability and computational weight. Photochemical reactions are treated in PLPM by means of the complex chemical mechanism SAPRC90 and four density reconstruction methods have been developed, based on the kernel density estimator approach, in order to obtain grid-free accurate concentrations.

Keywords: Photochemical pollution; Lagrangian chemical transport model; Grid-free model; Complex chemical mechanism; Kernel density estimator

1. Introduction

Despite of the progress observed in the last decades in the reduction of atmospheric pollution caused by many inert substances, photochemical pollution is still a major problem in several areas, both urban and rural, all over the world. The prediction of the concentration in air of secondary pollutants, like ozone (O_3), originated from photochemical reactions requires the use of complex mathematical models, with many more difficulties than those faced in the calculation of the dispersion of primary pollutants due to the complex relationships between ozone and its main precursors, NO_x and VOC. (Russell and Dennis, 2000) Due to the high non-linearity of photochemical reactions, the emission reductions needed to obtain the desired reduction in ozone concentration are not simple to quantify. Computer simulations using mathematical models can give an a priori evaluation of the emission reduction plans (e.g., Dentener et al., 2005; Zanini et al., 2004; Finzi et al., 2000). Mathematical models dealing with photochemistry are mostly based on the Eulerian approach, whereas a first

*Corresponding author. Tel.: +39 516098650; fax: +39 516098675.
E-mail address: monforti@bologna.enea.it (F. Monforti).

1352-2310/$ - see front matter © 2006 Elsevier Ltd. All rights reserved.
doi:10.1016/j.atmosenv.2006.07.046

prototype of photochemical Lagrangian particle model was introduced by Chock and Winkler (1994a, b). In this model each particle is marked with a chemical tag and a grid mesh for chemistry, varying both in space and in time, is superimposed to the calculation domain. The chemical reactions take place within the grid volume involving only the particles contained in it. The concentration of each species inside this chemical grid is calculated by counting the particles with a given tag and dividing the corresponding total mass by their partial volume (i.e., the grid volume occupied by the tagged particles). These concentrations are then given in input to the chemical module and the new mass of a particle is obtained multiplying the old mass times the ratio between the new and the old concentration for that species.

Following a similar approach, usually named Hybrid Eulerian–Lagrangian, Stein et al. (2000) have added a detailed non-linear Eulerian chemistry module implementing the CBM-IV mechanism (Gery et al., 1989) to a three-dimensional Lagrangian particle model and have applied it to regional scale modelling. On the contrary, Song et al. (2003a) have combined a Lagrangian dispersion algorithm with a time-dependent photochemical box model in order to obtain a reliable description of the evolution of ship plumes in the marine boundary layer. Recently, Song et al. (2003b) have developed a pure Lagrangian model with photochemical reactions. In this approach, each particle represents the geometrical centre of a puff with concentration assumed to be Gaussian with variances σ_j (with $j = x, y, z$). Values of σ_j are computed as the time integration of the velocity variances encountered over the history of the puff and particles are supposed to chemically react each other when they "intermix", i.e., they lay closer than twice their associated variances. Chemical reactions follow the photochemical mechanisms developed by Russell et al. (1988) and lead to particles mass change. Reaction efficiency between particles is supposed proportional to the amount of reactive species contained in the intermixing regions and to the turbulence intensity but it is inversely proportional to the diffusion time scale. This model has been validated on data collected for a power plant plume (Song et al., 2003b) and with the data obtained with the Southern Oxidants Study (Song and Park, 2004) giving satisfactory results.

In this paper, the chemistry module implemented in the Photochemical Lagrangian Particle Model (PLPM) is presented, discussed and tested. PLPM, developed starting from 1999 (Zanini et al., 2002; Sachero et al., 2004; Reggiani et al., 2005; Vitali et al., 2006), tries to make a step further in Lagrangian photochemical modelling since it uses a complex chemical mechanism and it is grid independent being based on a kernel density estimator. The model structure and the dynamic modules of PLPM have been extensively described and validated in Vitali et al. (2006) against the classical Kincaid and Copenhagen data sets and the performances of the different kernel methods in reconstructing ground concentrations were also assessed.

In this paper, a detailed description of the chemical module of PLPM is given and a set of tests involving density reconstruction efficiency in chemically active simulation context are described.

2. The PLPM Lagrangian treatment of photochemistry

Basic features of PLPM Lagrangian dynamics have been described in Vitali et al. (2006). PLPM contains also a chemistry module that can be switched on or off. If chemistry is active, each particle released is assumed to be composed by several pollutants. The number of pollutants carried by each particle changes in time since the chemical reactions may result in the production or loss of some species.

The condensed SAPRC90 chemical mechanism (Carter, 1990), lumping hydrocarbons in molecular groups according to their reactivity with the oxydril radical, is implemented in the current version of PLPM. Since PLPM is highly modular it should be relatively easy to incorporate in it more recent versions of the SAPRC mechanism (i.e., SAPRC93, SAPRC 97 or SAPRC99), or other mechanisms as the CB-IV (Gery et al., 1989) where hydrocarbons lumping is done according to the carbon bond type (e.g., single bond, double bond or carbonyl bonds).

Within PLPM, photochemical transformation of masses is activated at discrete time steps. The concentration of each species is computed at each particle's location using a product kernel density estimator:

$$c(x,y,z,t) = \sum_{i=1}^{n} \frac{m_i}{\lambda_x \lambda_y \lambda_z} d\left(\left|\frac{x_i - x}{\lambda_x}\right|\right) d\left(\left|\frac{y_i - y}{\lambda_y}\right|\right) d\left(\left|\frac{z_i - z}{\lambda_z}\right|\right). \quad (1a)$$

In PLPM the Epanechnikov kernel function

$$d(u) = \begin{cases} \frac{3}{4}(1-u^2), & |u| \leqslant 1, \\ 0, & |u| > 1 \end{cases} \quad (1b)$$

is employed while four methods fully described in Vitali et al. (2006) are available for setting the λ_i bandwidths. Briefly, the user can choose between four methods: PG (Particles-based, Global), PL1 (Particles-based, Local, 1-dimensional), PL3 (Particles-based, Local, 3-dimensional) and RL3 (Receptors-based, Local, 3-dimensional).

Concentration values are then input to the chemical mechanism, reactions take place and new concentration values for all the species, are computed at particle's location. Once the concentration field is transformed by photochemical reactions, the masses are redistributed back to particles: if $m_{i,j}$ and C_j are respectively the mass of the jth species carried by the ith particle and its concentration in the particle's location before the chemistry step, and $m'_{i,j}$ and C'_j are, respectively, the mass of the jth species carried by the same particle and its concentration in the particle's location after the chemistry, following Chock and Winkler (1994b) it is assumed that

$$m'_{i,j} = m_{i,j}\frac{c'_j}{c_j}. \quad (2)$$

This equation allows masses of each species to be modified according to the variation of their concentrations. It cannot be applied if the species concentration before the chemistry step is zero. In such a situation m'_j is calculated as

$$m'_{i,j} = m_{i,\mathrm{tot}}\frac{c'_j}{c'_{\mathrm{tot}}}, \quad (3)$$

where $m_{i,\mathrm{tot}}$ is the total mass of the ith particle and c'_{tot} is the sum of c'_j for all species considered by the chemical mechanism. It is worth noticing as this approach reassigns particles masses after chemical reactions in a way independent of the kernal applied for the computation of concentrations and does not move particles from their pre-chemistry location.

2.1. Computational costs

The computational cost of the chemistry module depends on two factors:

- the computational time needed by the different kernel methods and, more specifically, by the bandwidths calculation methods employed,
- the computational time needed for computing the concentration field in each particle's location.

As for bandwidths setting, referring to the extensive kernel description contained in Vitali et al. (2006), computational times can be easily linked to the number of particles if one considers that, given a set of N points in space, the number of operations needed to compute their reciprocal distances is about $3N(N-1)/2$ whereas sorting N numbers in ascending or descending order needs a number of operations equal to $N\log_2 N$.

Table 1 shows the overall scaling properties of computational times for the kernels tested for PLPM: kernel PG shows a clear computational advantage, as it does not need any neighbourhood definition and its computational time is almost linear with particles number; on the contrary, other kernels depend on the square of the particles number (or the product of particles and receptors number in the case of RL3). For PLPM applications involving some thousands of particles, like the ones described in this paper and in Vitali et al. (2006), bandwidths setting computational times are afford-

Table 1
Number of operations needed (columns 2–4) and overall scaling of computational times (column 5) of kernels as a function of particles number (N_p) and receptors number (N_r)

Kernel	Distance between particles or between particles and receptors	Sorting(s)	Other operations	Overall scaling
PG	—	$3 \times N_\mathrm{p}\log N_\mathrm{p}$ [a]	$3 \times N_\mathrm{p}$ [b]	$N_\mathrm{p}\log N_\mathrm{p}$
PL3	$3 \times N_\mathrm{p}(N_\mathrm{p}-1)/2$	$N_\mathrm{p}^2\log N_\mathrm{p}$	—	$N_\mathrm{p}^2\log N_\mathrm{p}$
PL1	$3 \times N_\mathrm{p}(N_\mathrm{p}-1)/2$	$3 \times N_\mathrm{p}^2\log N_\mathrm{p}$	—	$N_\mathrm{p}^2\log N_\mathrm{p}$
RL3	$3 \times N_\mathrm{p}(N_\mathrm{r}-1)/2$	$\mathrm{N_r} \times N_\mathrm{p}\log N_\mathrm{p}$	—	$\mathrm{N_r} \times N_\mathrm{p}\log N_\mathrm{p}$

[a] Computation of interquartile ranges.
[b] Computation of σ_j.

able for all kernels on an usual PC. On the contrary, if simulations involving higher particles numbers are planned, more computational resources are needed by nearest neighbourhood-based kernels PL1, PL3 and RL3.

Anyway, a conspicuous share of computation weight is normally expected to be employed in the density reconstruction. Indeed, regardless of the kind of kernel employed, a computational time proportional to N_p^2 is needed in order to apply the basic kernel reconstruction Eq. (1a) and (1b) in each particle's location.

3. Testing the chemistry module

While the kernel method is not novel in air pollution dispersion modelling, its application to Lagrangian photochemistry is a novel one and it should be deeply tested for both numerical stability and results reliability before being fully implemented in the framework of a mature dispersion model. For this reason a number of tests on the module were performed, allowing the PLPM developers to become aware of a number of strong and weak points of each of the approaches employed.

3.1. Density estimation assessment

A first set of tests has been set up to evaluate the performances of the density reconstruction algorithms in some simple static situation before moving to full chemical treatment: N particles with the same mass were placed in space according to a certain (known) density distribution $c(x,y,z)$ and kernel density reconstruction methods are employed to compute the estimated density distribution $\hat{c}(x,y,z)$ by means of Eq. (1a) and (1b). With a "perfect" density reconstruction one should obtain $c(x,y,z) = \hat{c}(x,y,z)$ and performances of density reconstruction methods can be assessed evaluating differences between the theoretical and the estimated densities.

3.1.1. Uniform distribution

The first density reconstruction test involved an uniform concentration density $c(x,y,z) = 125\,\mu g/m^3$. Fig. 1 shows average value of $\hat{c}(x,y,z)$ as a function of particle number N generated: as expected density estimation improves with growing particle numbers and all kernels seem to tend asymptotically to the theoretical average value, with PL1 reaching it for $N \sim 2000$ and then oscillating. All kernels overestimate density and tend to the optimal value from above but PL1 and PL3 are clearly better performing than PG and RL3.

In Fig. 2 the value of the standard deviation (SD) between the estimated and theoretical concentration:

$$\mathrm{SD} = \sqrt{\frac{\sum_{i=1}^{N}[c(x_i,y_i,z_i) - \hat{c}(x_i,y_i,z_i)]^2}{N-1}} \quad (4)$$

is shown (x_i, y_i, z_i) being particles' Cartesian coordinates. Three kernels, namely PL3, PG and RL3 show a performance improvement for growing N and seem to tend to the "ideal" value (i.e., SD = 0),

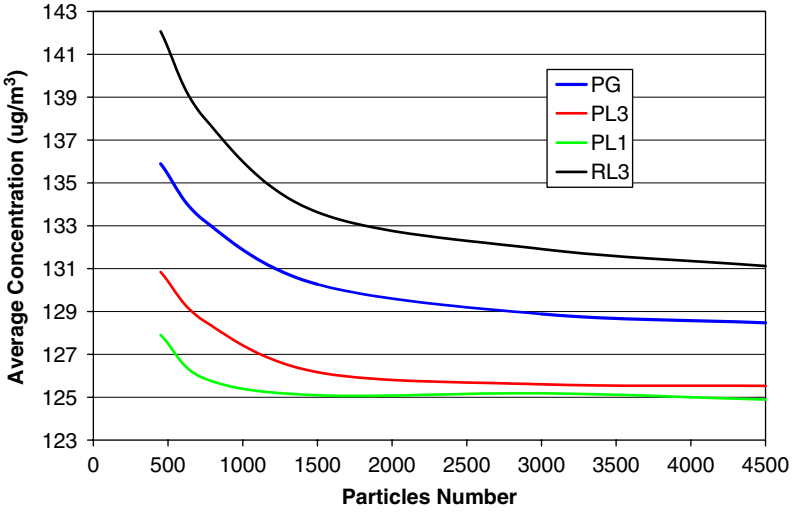

Fig. 1. Average value estimates of a uniform concentration of 125 μg/m^3 as a function of the number N of particles employed for different kernel types.

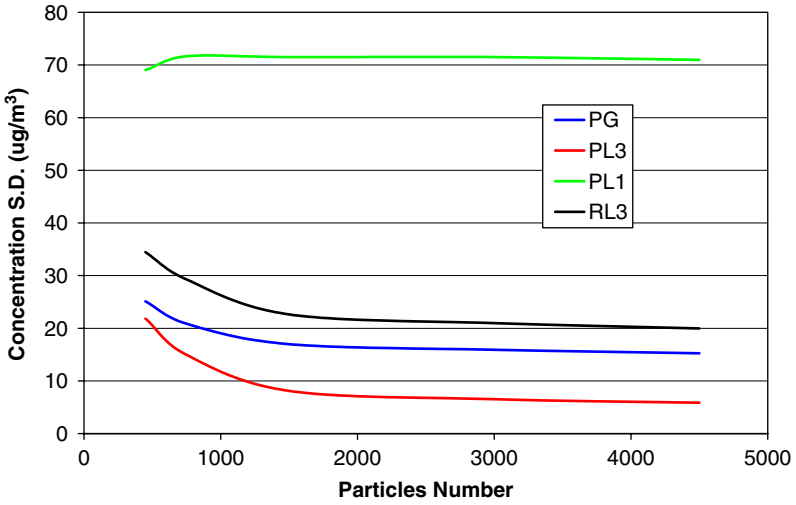

Fig. 2. Standard deviation estimates of an uniform concentration of 125 μg/m^3 as a function of the number of particles N for different kernel types.

though slower than what observed in the case of average values. On the contrary, for PL1 a much higher value of SD, nearly independent from N, is found. In other words, PL1 is found to be the best performing method to reconstruct an uniform density, as far as average value is concerned, but its estimates suffer of high variability not likely to improve increasing the number of particles employed.

3.1.2. Gaussian plume distribution

In another test a set of $N = 4500$ particles were generated miming a perfect Gaussian plume in the positive x direction, with perfect flat terrain reflection:

$$c(x,y,z) = \frac{C_0}{\sigma_y \sigma_z} \exp\left(-\frac{y^2}{2\sigma_y^2}\right) \times \left[\exp\left(-\frac{(z-z_s)^2}{2\sigma_y^2}\right) + \exp\left(-\frac{(z+z_s)^2}{2\sigma_z^2}\right)\right], \quad (5)$$

where the source height z_s was set equal to 200 m, σ_y and σ_z follow the Pasquill–Gifford curves for stability class D (neutral atmosphere) and C_0 is a normalization coefficient depending of the number and the mass of particles generated. The "ideal" plume generated is shown in Fig. 3. The density estimation $\hat{c}(x,y,z)$ was computed and compared with theoretical Gaussian density on a number of receptor sets. Fig. 4 shows estimated and theoretical density profiles on 4 half arcs, laying from -90° to 90°, at the ground level and centred in the source position with increasing radius (namely 1000, 2000, 4000 and 7000 m). Fig. 5 shows estimated and theoretical concentrations along 4 vertical profiles orthogonal to x-axis at increasingly distances form the source (again 1000, 2000, 4000 and 7000 m) and Fig. 6 shows estimated and theoretical concentrations on the plume axis, i.e. along positive x-axis at 200 m height.

Figs. 4–6 confirm as estimates based on different kernel methods can be considerably different, depending on the receptors location. Both arcs and profile show that there are two kernels, namely PL3 and RL3, leading to "smooth" density fields, a kernel leading to strongly irregular density fields (PL1), especially far away from the source, with PG leading to a slightly irregular field. At distances from the source smaller than 2000 m all kernels tend to overestimate ground concentration whereas at 7000 m almost all kernels lead to a slight underestimation. Vertical profiles (Fig. 5) show also as the kernels distribute differently the particles mass in the vertical direction: PL3 and RL3 tend to disperse the mass too much, so leading to a systematic underestimation in the region between 100 and 300 m of height; the same kernels tend to overestimate the concentration in the vertical distribution tailes, i.e., below 100 m and above 300 m. On the contrary, PL1 leads to a very narrow concentration distribution in the vertical direction close to the source, but it suffers of a rapid degradation

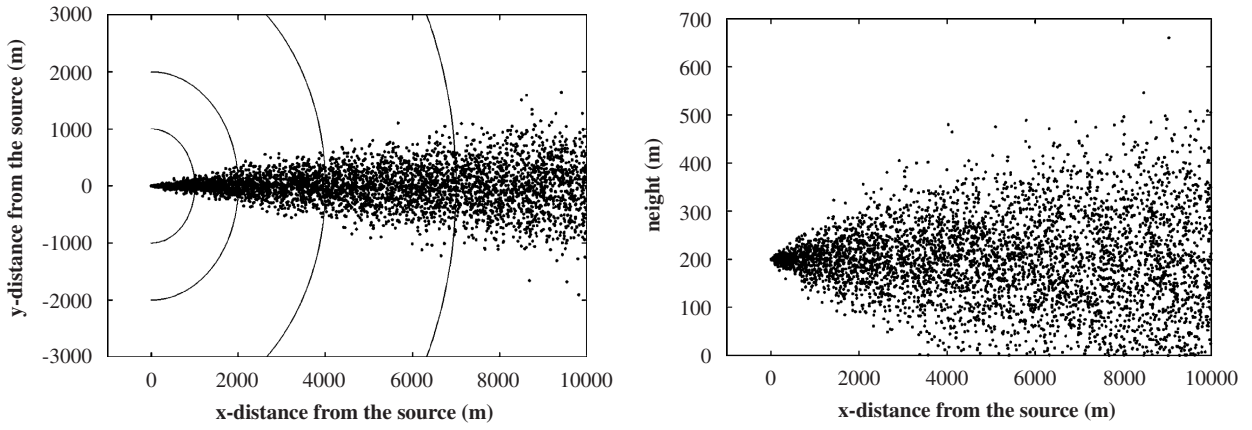

Fig. 3. *X–Y* (left) and *X–Z* (right) projection of the ideal Gaussian plume in neutral dispersion conditions generated for testing kernel performances. 1000, 2000, 4000 and 7000-m radius receptor arcs used for density reconstruction assessment are also shown.

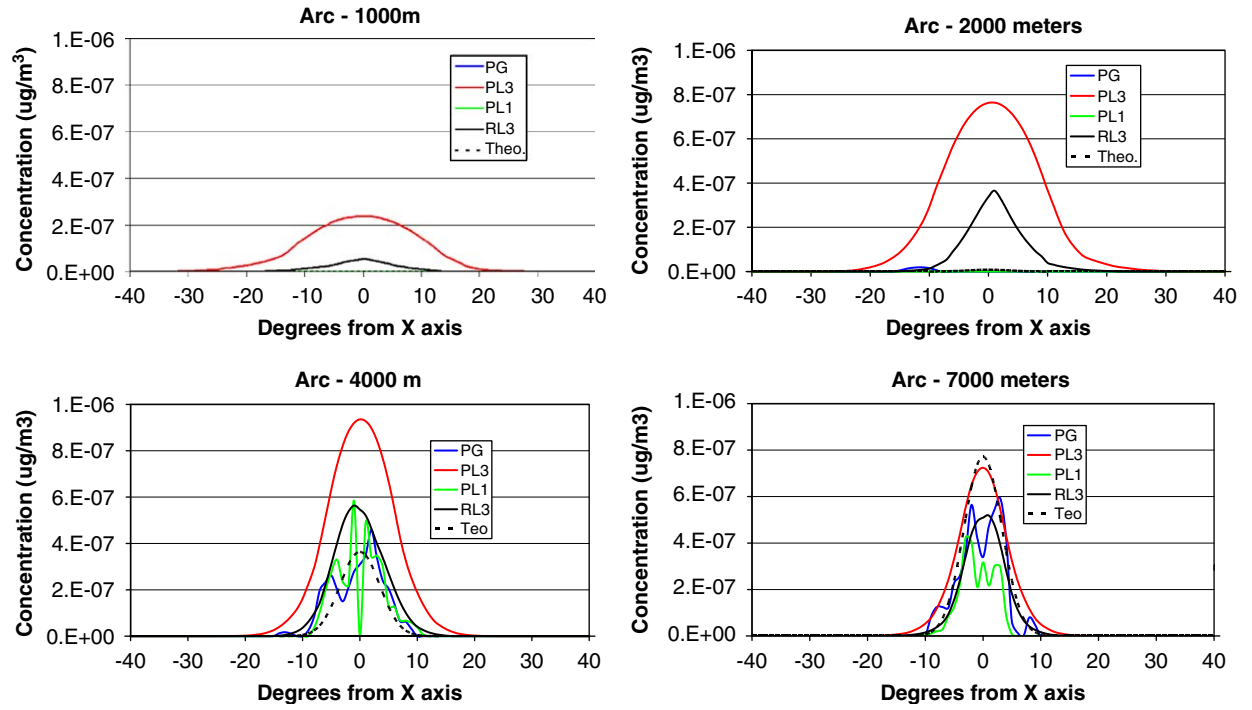

Fig. 4. Theoretical and reconstructed concentration profiles (in $\mu g/m^3$) on the 1000-m (top left), 2000-m (top right), 4000-m (bottom left) and 7000-m radius (bottom right) ground receptor arcs.

moving away. As for PG, the selected tests seem to indicate it as a good compromise between smoothness and correct evaluation. Fig. 7 shows maps of ground concentration obtained with different kernels for the perfect Gaussian particles plume described by Eq. (5) [left] and for the same plume rotated by 45° in anticlockwise direction [right]. For reconstruction methods based on local approach (i.e., PL1, PL3 and RL3) the ground density pattern does not change substantially whereas the density pattern obtained with PG is clearly different in the two cases. The reason for this behaviour is that in PG bandwidths are computed on the basis of *global* components of standard deviation of particle

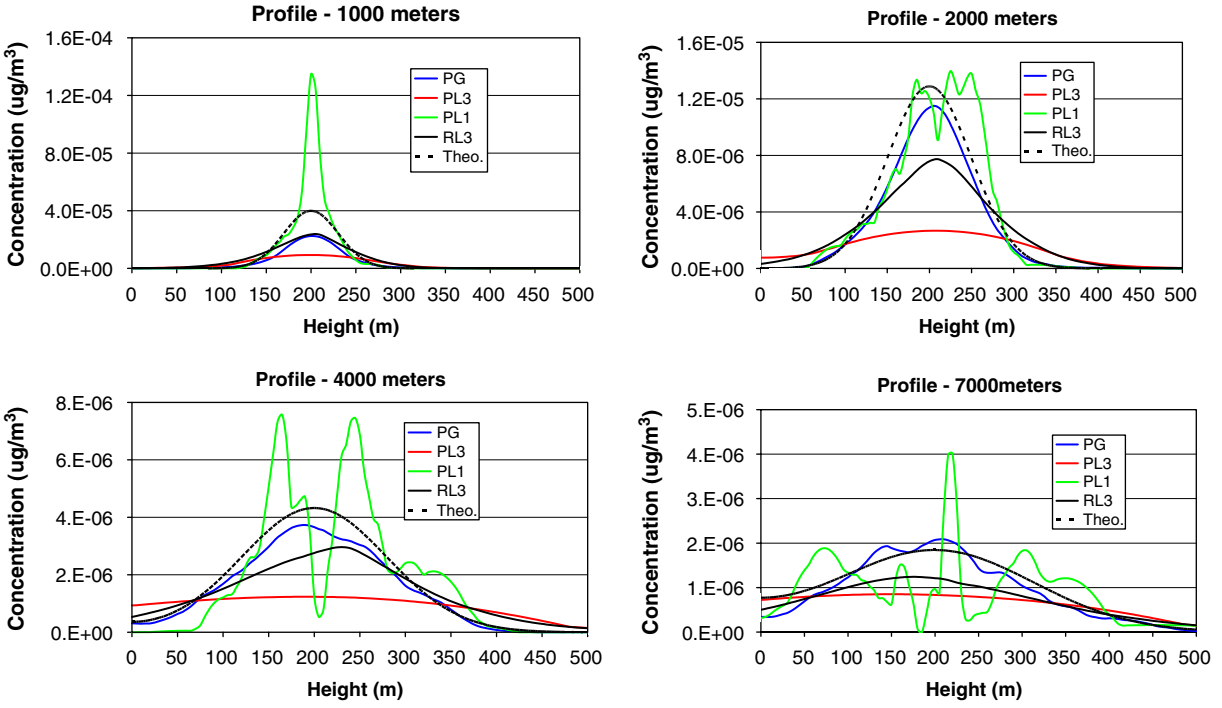

Fig. 5. Theoretical and reconstructed concentration profiles (in μg/m^3) on the 1000-m (top left), 2000-m (top right), 4000-m (bottom left) and 7000-m (bottom right) downwind vertical receptor lines.

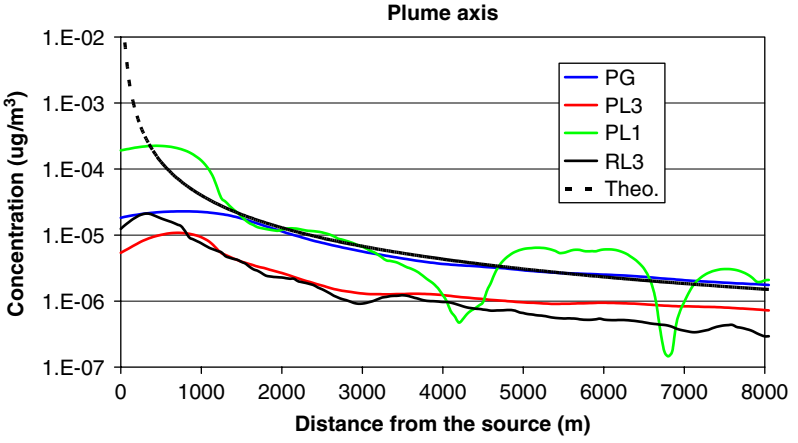

Fig. 6. Theoretical and reconstructed concentration profiles (in μg/m^3) on the receptors line located in the plume axis.

positions following the formula (De Haan, 1999):

$$\lambda_j = \alpha A(K) n^{-1/7} \min\left(\sigma_j, \frac{R_j}{1.34}\right)$$

$$\text{with} \quad j[= x, y, z], \tag{6}$$

where n is the particles number and α and $A(K)$ are constants.

In the special case of a plume with axis parallel to x-axis (Fig. 3) one has $\sigma_x \gg \sigma_y$ and then $\lambda_x \gg \lambda_y$ from Eq. (6); in such a situation, particles' mass is spread strongly asymmetrically with preference for x-direction, as it is evident from Fig. 7(a), leading to a quite irregular concentration pattern. On the contrary, if the plume axis is rotated by 45°, one has $\sigma_x \approx \sigma_y$ and then $\lambda_x \approx \lambda_y$ for each particle and

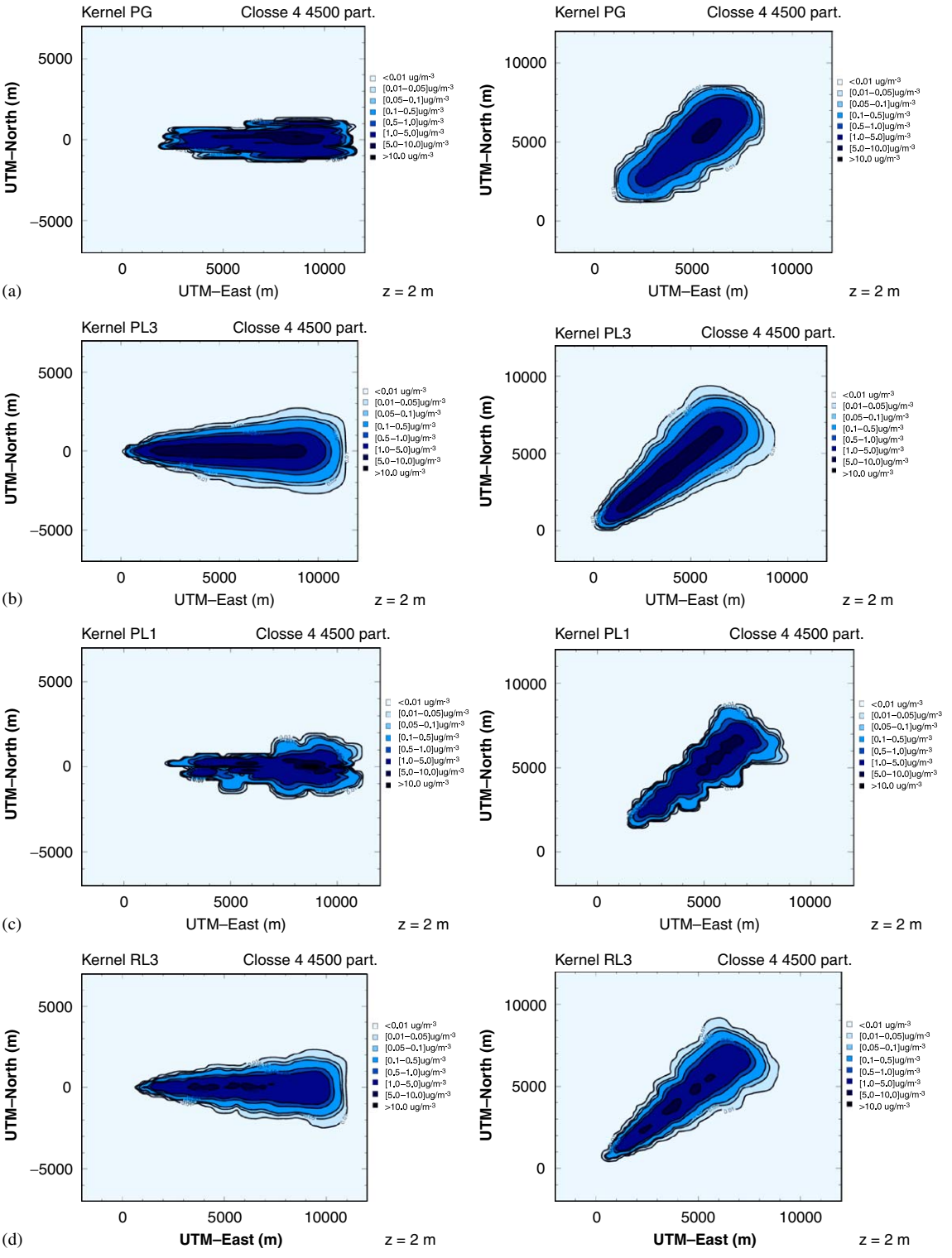

Fig. 7. Ground concentration maps obtained with different kernels for the ideal Gaussian plume shown in Fig. 3 and for the same plume rotated by 45° in the horizontal plane.

particles mass is spread mass in a broadly symmetrical way and resulting concentration pattern is noticeably smoother. Local-based kernels are exempt from this rotational effect as they consider only the particles neighbourhoods when setting bandwidths, i.e., a particles subset that is likely to have a more symmetrical shape than the whole plume, leading to $\lambda_x \approx \lambda_y$ regardless of the whole plume position in respect to the coordinate axis.

3.2. Photochemical evolution of a box

On the basis of similar tests reported in literature (Seinfeld and Pandis, 1998) a further test was developed in order to evaluate the impact on the chemical module of PLPM of the ability of different kernels in density reconstruction.

Chemical evolution taking place in a box initially containing an homogeneous mixture of NO (0.1 ppm), NO_2 (0.01 ppm), HCHO (0.1 ppm) RCHO (0.1 ppm) and hydrocarbons (0.1 ppm) was simulated by means of PLPM: 2000 particles were placed randomly in a $1000 \times 1000 \times 400$ m wide box, each particle having the same mass and chemical composition. No active and boundary sources were present and the model was run with constant solar radiation to simulate 5 h of chemical evolution in a static way (i.e., particles were maintained at rest).

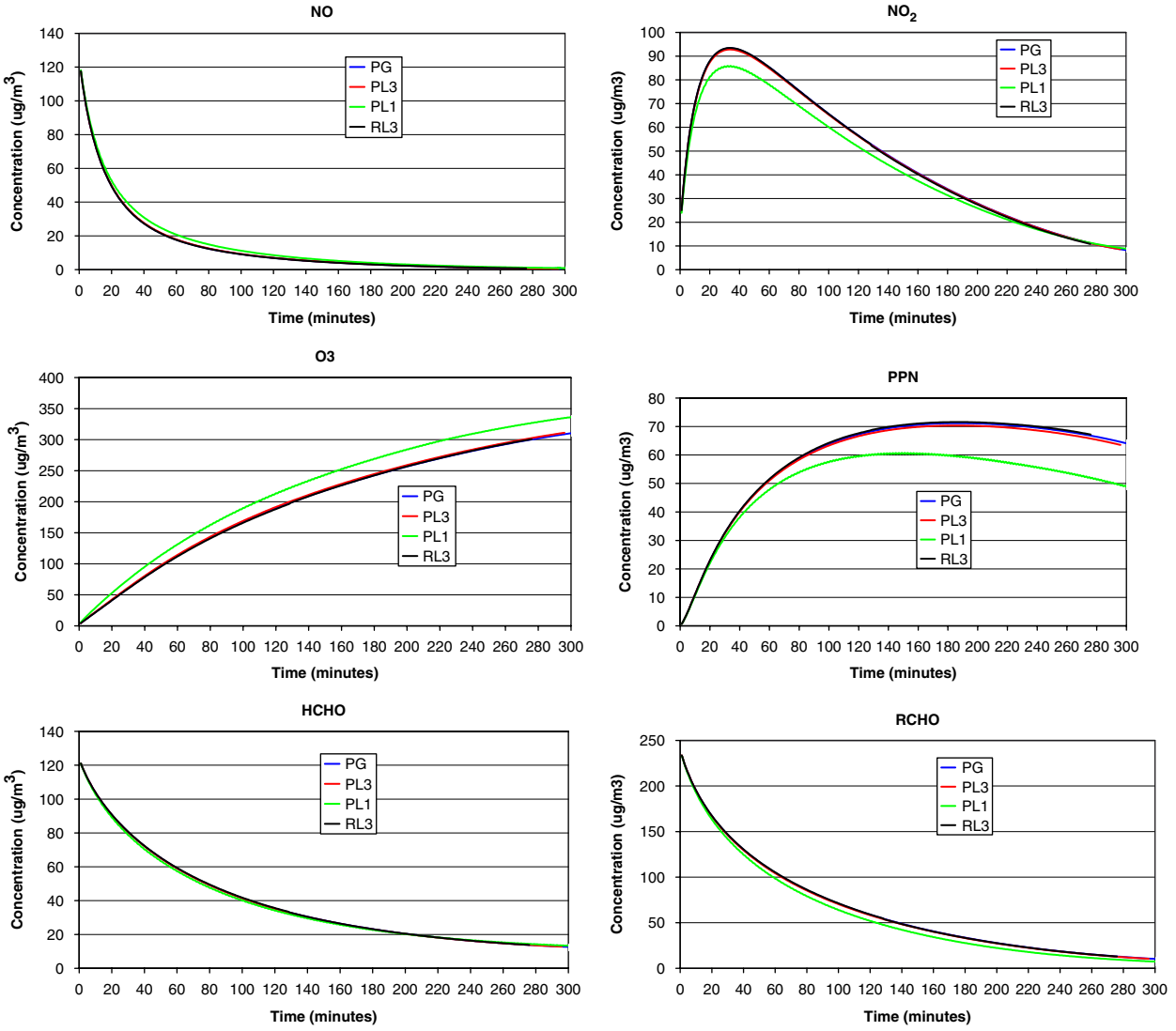

Fig. 8. Concentration evolution of NO (top left), NO_2 (top right), O_3 (middle left), PPN (middle right), HCHO (bottom left) and RCHO (bottom right) in an uniform box with initial concentrations described in text obtained with different kernel methods.

Fig. 8 shows the evolution of the average box concentration of some chemical species as obtained with different kernel reconstruction methods. All the kernels give broadly the same results, with PL1 leading to slightly different concentrations (higher or lower depending of the compound considered). The overall agreement with chemical behaviour expected (Seinfeld and Pandis, 1998) is very encouraging for the model suitability in reproducing complex chemical evolution and it is a solid basis for future model validations involving chemically active compounds.

Besides their ability in computing average concentrations, kernel methods were also checked for their stability: Fig. 9 shows time evolution of $SD_j/\bar{m}_j$ where $\bar{m}_j = \sum_{i=1}^{N} m_{i,j}$ and

$$SD_j = \sqrt{\frac{\sum_{i=1}^{N}(m_{i,j} - \bar{m}_j)^2}{N-1}}$$

are, respectively, the average value and the standard deviation of the $m_{i,j}$, i.e. the mass of jth chemical compound carried by each of the N particles.

Lower values of this indicator are preferable as they indicate more uniform concentration fields whereas high values imply large local concentration irregularities likely to end up in a numerical "blow up". Different chemical species can show values of

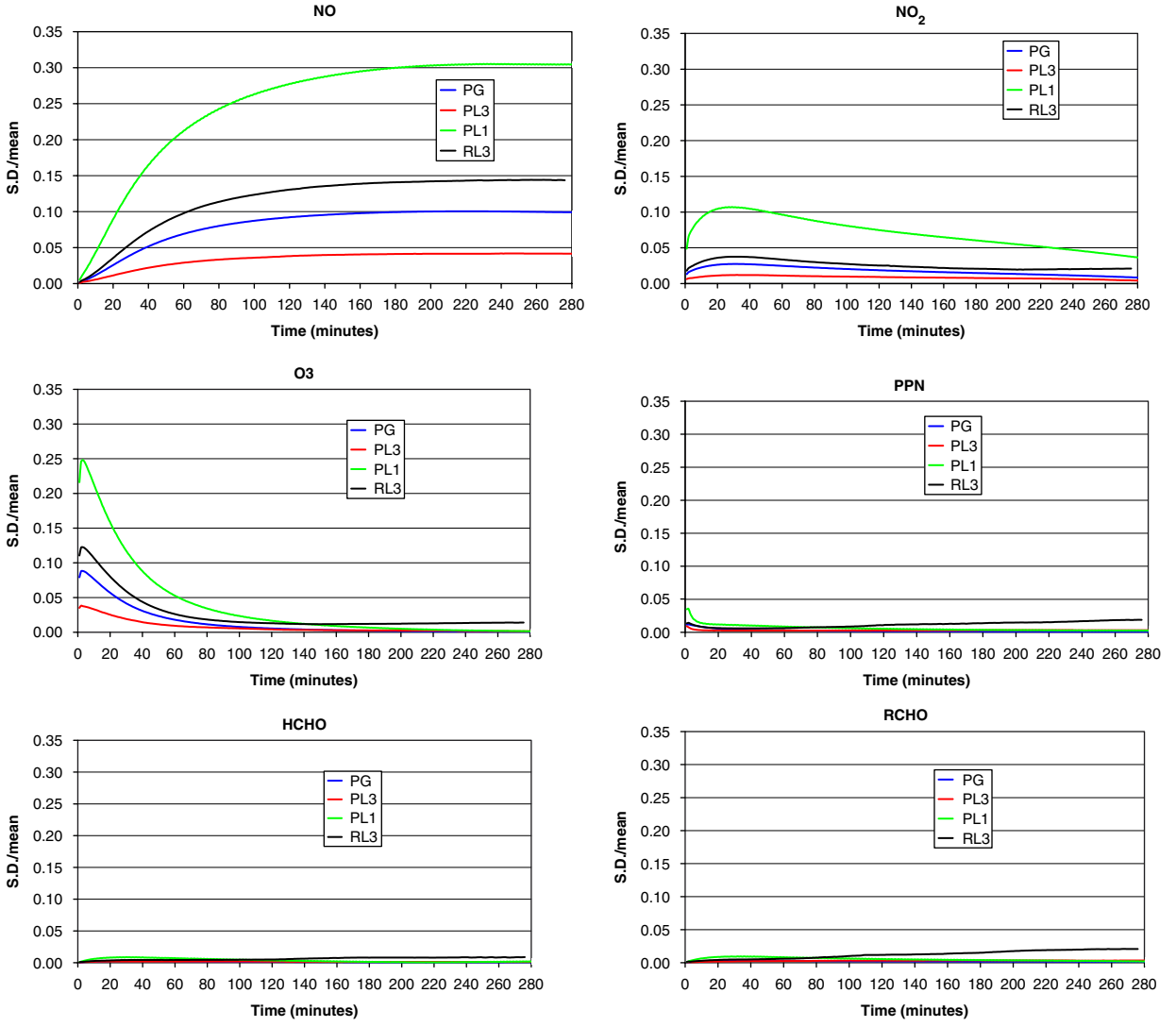

Fig. 9. Values of SD/m obtained for the same species of Fig. 8 with different kernel methods.

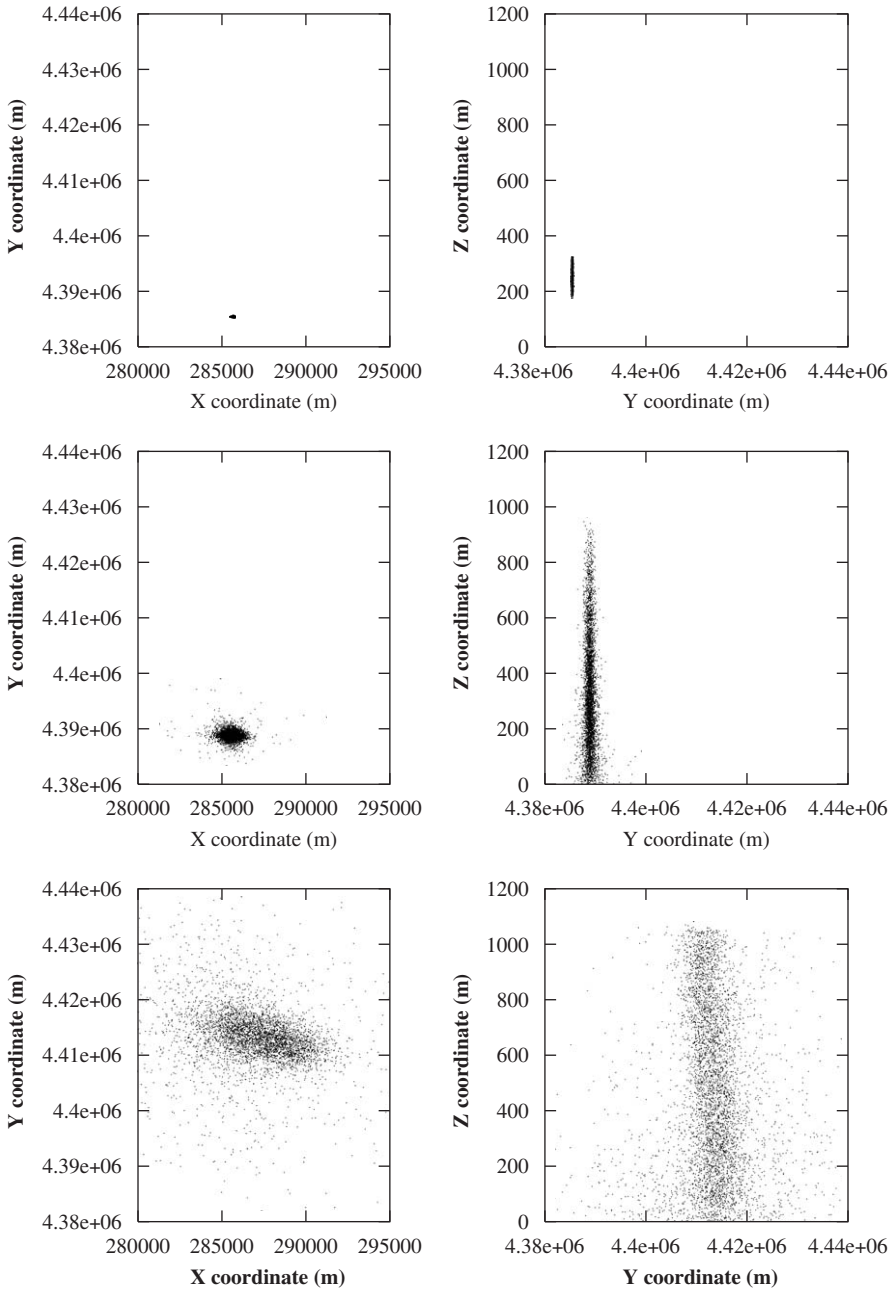

Fig. 10. *X–Y* (left) and *Y–Z* (right) projections showing the dynamical evolution at 9:01 (top), 9:10 (middle) and 10:00 (bottom) of a puff emitted at 9.00 a.m of 25 May 1981 in the Kincaid experiment domain.

SD/m different also by a factor of 10, depending on how the reactions in which they are involved are sensitive to unavoidable density irregularities: between the species shown, NO, NO_2 and O_3 have the lower stability, whereas PPN, HCHO and RCHO show a lower density fluctuations. Furthermore, it is evident as different kernels methods can also lead to considerably different chemical stability, with PL3 kernel generally performing better than the other methods, confirming its suitability in dealing with uniform concentrations shown also in Fig. 2.

3.3. Photochemical evolution of a puff

Finally, a test for the stability and reliability of the kernel approach in a simulation involving both

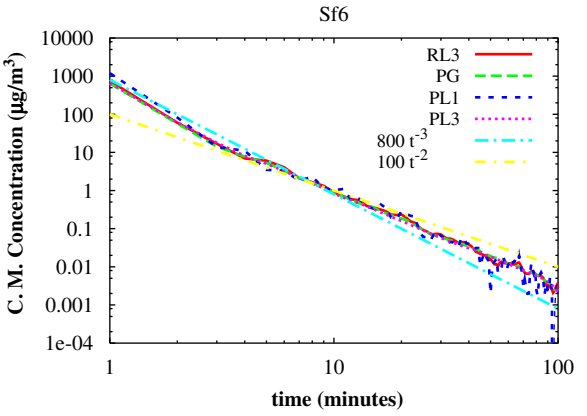

Fig. 11. Concentration of SF_6 (inert) computed with the four kernels in the puff centre of mass as a function of time.

dynamical and chemistry modules of the model has been set up. The domain, meteorology and source features (stack height, emission velocity and temperature) of the Kincaid experiment for 25 May 1981 at 9.00 a.m. were employed. In a first test, a puff composed by 5000 particles each carrying 0.12 g of inert pollutant SF_6 was emitted. In a second test an a chemically active puff, also composed by 5000 particles each carrying 0.12 g of a mixture of NO, NO_2, HCHO, RCHO and hydrocarbons was also emitted at the same time and place, the ratio between compound initial masses being the same of the case study treated in Section 3.2. As in the present version of PLPM the particles dynamics does not depend on their masses, the two puffs behaves absolutely identically from the point of view of particles positions in different time steps (the two simulations were run with the same random number seed, in order to obtain the same realisation of the stochastically varying turbulence parameters). On the contrary, in the chemically active simulation total particles masses changes in time together with the number and the amount of chemical compounds carried by each particle. Fig. 10 shows 3 representations of the puff 1, 10 and 60 min after the release. The puff moves from the source in northern direction while dispersing in all directions. At about 10 min from the simulation start, the plume has dispersed fully in the vertical direction and in next time steps, particles tend to well mix in the boundary layer. Particles begin to exit from the domain about 60 min after the simulation start and after about 100 min only half of the particles remains inside the domain, coherently with a domain size of 50 km from the source in northern direction and an average wind speed of about 14 m/s at the puff average height. Because of this "border effect", the following results have to be considered less and lesser significant with time after 60 min and no results will be shown for simulation time longer than 100 min.

Fig. 11 shows the concentration of SF_6 (inert) computed with the four kernels in the puff centre of mass as a function of time. It is interesting to notice as the concentration decreases roughly in proportion to t^{-3} during the first 10 min, as expected (Seinfeld and Pandis, 1998) before the boundary layer saturation (see Fig. 10). On the contrary, after 10 min, the concentration decreasing is less rapid, the curve slope moving closer to t^{-2}. All the kernels seem to correctly reproduce the same puff concentration evolution, with PL1 showing a slightly more instable behaviour.

Fig. 12 shows the concentrations in the centre of mass of the chemically reactive plume for the same compounds computed analysed in Figs. 8 and 9. It is clear how the concentration of all the compounds decreases mainly because of puff dynamical dispersion and all the kernel methods can easily follow the puff evolution, again with PL1 and, to a lower extent, RL3 showing a somewhat more irregular behaviour.

Anyway, even if the centre of mass concentration of all the compounds decrease for clear dynamic reasons, one has to notice as different compounds show different decreasing rates because of different chemical behaviour. This aspect is more emphasised if one compares the concentration of each compound with the concentration of SF_6 in the inert case, both normalised to unity at $t = 1$ min (Fig. 13—only results for kernel PL3 shown). For O_3 and PPN concentration decreases slower (or much slower in the case of O_3) than the inert meaning that these compounds are produced by chemical reactions taking place inside the puff, that is obvious in this case, as the two compounds were not present in the initial conditions. On the contrary NO_2 decreases more rapidly than the inert reference, meaning it is mainly consumed by the chemical reactions taking place inside the puff. The other compounds show a more or less inert-like behaviour, with dynamical features fully prevailing on chemical aspects.

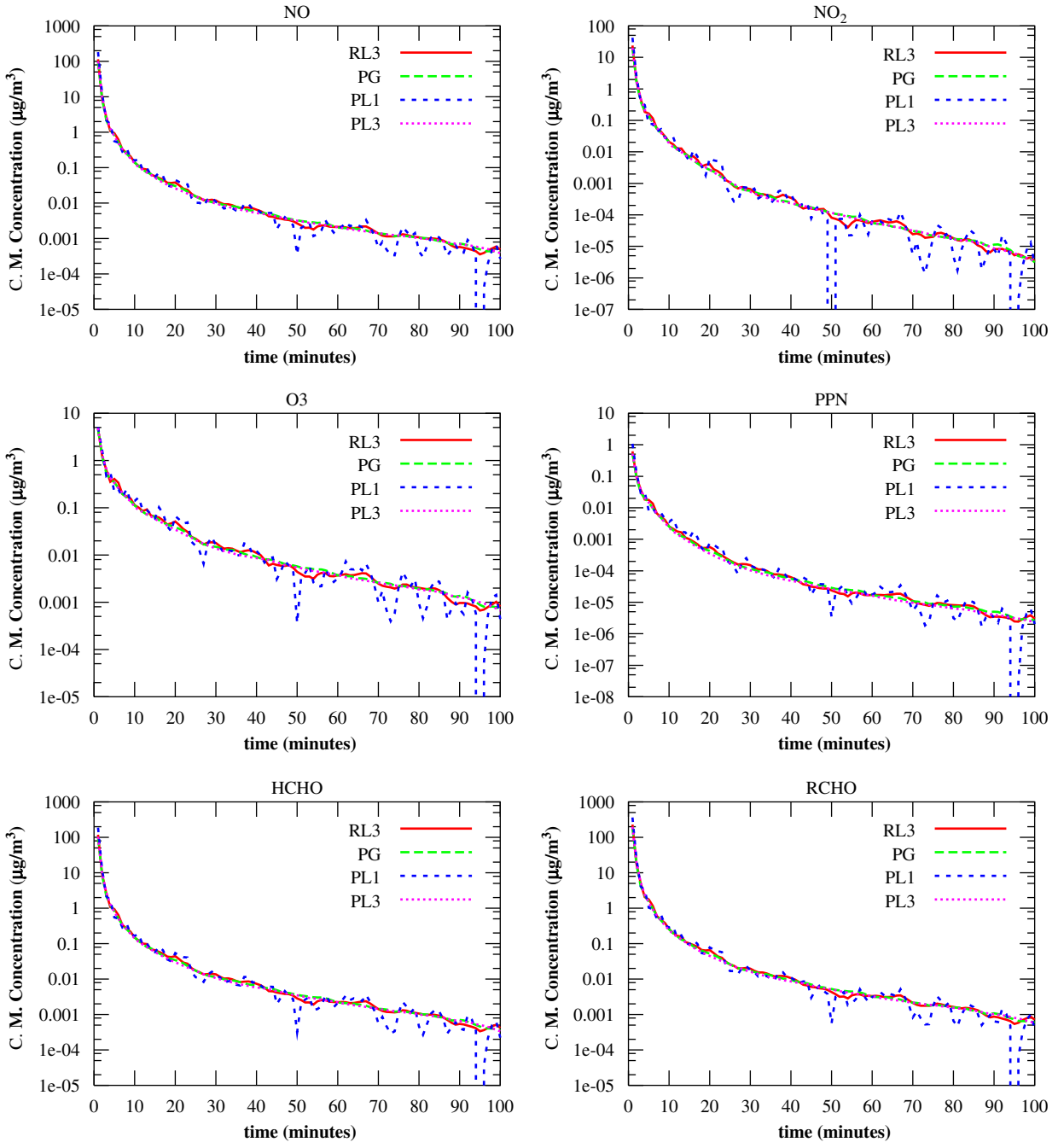

Fig. 12. Concentration of NO (top left), NO_2 (top right), O_3 (middle left), PPN (middle right), HCHO (bottom left) and RCHO (bottom right) computed with the four kernels in the puff centre of mass as a function of time.

3.4. Summary of kernels performances

On summary, preliminary tests performed allowed to identify strong and weak points for the tested kernels:

- PG seems to give best performances in reconstructing Gaussian plume density (Figs. 4–6) but it is not independent from coordinates axis position (Fig. 7) and it leads to some degree of irregularity when reconstructing uniform concentrations (Figs. 2 and 9).

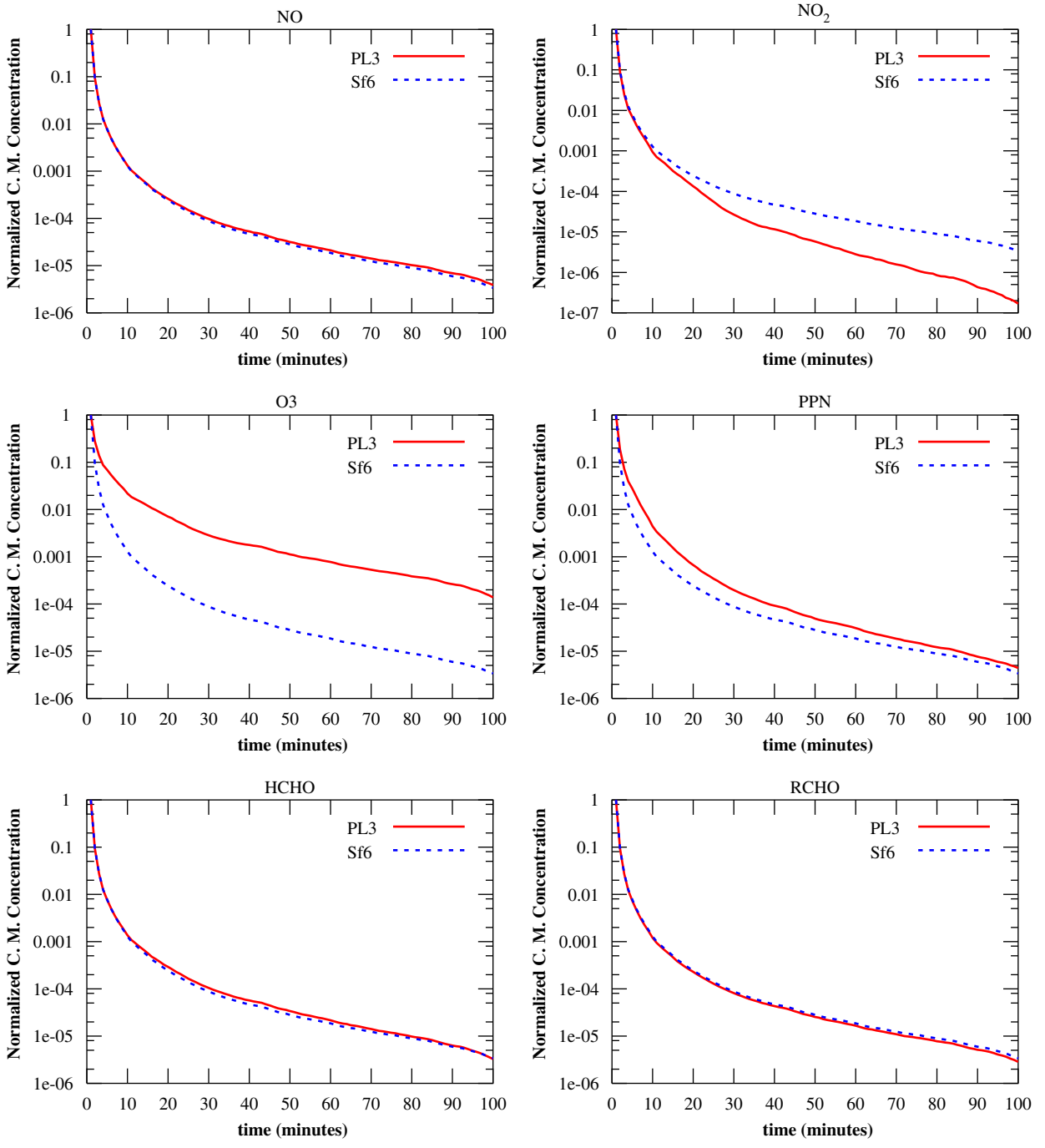

Fig. 13. Comparison between the normalised concentrations in the puff centre of mass for the same six chemically active compounds shown in Fig. 12 and the inert pollutant shown in Fig. 11 (Concentration normalised at $t = 1$ min). Only results obtained with PL3 kernel are shown.

- PL1 reconstructed density fields are by far the most irregular ones even if it seems to give best reconstruction close to the source (Fig. 6) and best average values when tested on uniform concentrations (Fig. 1).
- RL3 gives concentration fields quite smooth (Fig. 7) but it tends to spread too much particles mass in space (i.e., bandwidths are too large) leading to some underestimation inside the plume (Figs. 5 and 6) and an overall overestimation of

ground concentrations, especially close to the source (Fig. 4).

- PL3 gives the most smooth concentration fields (Fig. 7) but it shows the worst tendency to overspread particles mass in space (Figs. 4–6); when reconstructing uniform concentration both in the inert and in the chemically active case; PL3 gives the best results as far as homogeneity is concerned (Figs. 2 and 9).

Given these results, it evident as each kernel shows both positive and negative aspects, and none of them can be pointed as the "best" one. Furthermore, all the kernels show comparable skills in reproducing the test case of the chemically active puff (Figs. 11–13), except for PL1 showing a higher degree of instability.

4. Discussion and conclusions

The chemical module of a first prototype of a fully Lagrangian photochemical particle model, PLPM, has been presented and discussed. The treatment of photochemistry in PLPM is based on a density reconstruction algorithm implementing the kernel methodology. Such an approach allows to overcome the problem of box dimensions setting encountered when dealing with box counting density estimator and leads to fully grid-free computations. As of bandwidths setting, four methods are available in PLPM, one based on global features of particles distribution and three considering local distribution features by means of the definition of a particle (or receptor) neighbourhood. Kernel performances in reconstructing simple test densities have been compared both from the point of view of results precision and computation time. Furthermore, the chemical module of PLPM has been tested in the simple cases of a box containing uniform concentrations of photochemically reactive compounds and of a chemically active puff dispersing in the Boundary Layer. Kernel reconstruction methods have been assessed once again on the basis of their suitability to be coupled with a chemistry simulation. While the preliminary tests presented here are simple, they suggest that Lagrangian particle models can be a valid approach in the future for modelling photochemical pollution, if integrated with kernel-based density reconstruction methods, as all results obtained are very encouraging regarding both reliability and numerical stability. It is also worth noticing as the specific algorithms currently implemented in PLPM and presented here are not the only possible ones, and room is left for successive improvements or changes, depending on the outcomes of the full validation of the model. As an example, the use of particles composed by many pollutants has not been tested to be preferable to the approach of generating particles each composed by one substance. Another possible improvement, not investigated at the moment, could consist in introducing a different algorithm to reassign back particle masses after chemical reactions without the constraint of conserving particles positions. Such an approach would have the advantage that "free" particles are likely to map in better detail steep space variations of pollutants concentrations, but, at the moment, has showed to be very delicate from the point of view of computational stability and quite demanding from the point of view of computational resources.

Acknowledgements

Contribution of Gianni Pagnini was granted under a contract financed by Regione Emilia-Romagna in the frame of the project "Laboratorio LaRIA".

References

Carter, W.P.L., 1990. A detailed mechanism for the gas-phase atmospheric reactions of organic compounds. Atmospheric Environment 24A, 481–518.

Chock, D.P., Winkler, S.L., 1994a. A particle grid air quality modelling approach, 1: the dispersion aspect. Journal of Geophysical Research D 99, 1019–1031.

Chock, D.P., Winkler, S.L., 1994b. A particle grid air quality modelling approach, 2: coupling with chemistry. Journal of Geophysical Research D 99, 1033–1041.

de Haan, P., 1999. On the use of density kernels for concentration estimations within particle and puff dispersion models. Atmospheric Environment 33, 2007–2021.

Dentener, F., Stevenson, D., Cofala, J., Mechler, R., Amann, M., Bergamaschi, P., Raes, F., Derwent, R., 2005. The impact of air pollutant and methane emission controls on tropospheric ozone and radiative forcing: CTM calculations for the period 1990–2030. Atmospheric Chemistry and Physics 5, 1731–1755.

Finzi, G., Silibello, C., Volta, M., 2000. Evaluation of urban pollution abatement strategies by a photochemical dispersion model. International Journal of Environment and Pollution 14, 616–624.

Gery, M.W., Whitten, G.Z., Killus, J.P., Dodge, M.C., 1989. A photochemical kinetics mechanism for urban and regional scale computer modelling. Journal of Geophysical Research D 94, 12925–12956.

Reggiani, R., Vitali, L., Monforti, F., 2005. Validation of the PLPM model on the Copenhagen data set. In: Proceedings of Fifth Urban Air Quality Conference, Valencia, Spain, 29–31 March 2005.

Russell, A., Dennis, R., 2000. NARSTO critical review of photochemical models and modeling. Atmospheric Environment 34, 2283–2324.

Russell, A., McCue, K.F., Cass, G.R., 1988. Mathematical modelling of the formation of nitrogen-containing air pollutants, 1: evaluation of an Eulerian photochemical model. Environmental Science and Technology 22, 263–271.

Sachero, V., Vitali, L., Monforti, F., Zanini, G., 2004. PR-PLPM (Plume Rise Photochemical Lagrangian Particle Model): formulation and validation of the new plume rise scheme. In: Proceedings of the Ninth International Conference on Harmonisation within Atmospheric Dispersion Modelling for Regulatory Purposes, Garmisch-Partenkirchen, Germany, June 2004.

Seinfeld, J.H., Pandis, S.N., 1998. Atmospheric Chemistry and Physics. Wiley, New York.

Song, C.-K., Park, S.-U., 2004. Effects of the intermixing process between the Lagrangian particles on the estimation of concentration in the Lagrangian particle dispersion model. Atmospheric Environment 38, 3765–3773.

Song, C.-H., Chen, G., Davis, D.D., 2003a. Chemical evolution and dispersion of ship plumes in the remote marine boundary layer: investigation of sulphur chemistry. Atmospheric Environment 37, 2663–2679.

Song, C.K., Kim, C.-H., Lee, S.-H., Park, S.-U., 2003b. A 3-D Lagrangian particle dispersion model with photochemical reactions. Atmospheric Environment 37, 4607–4623.

Stein, A.F., Lamb, D., Draxler, R.R., 2000. Incorporation of detailed chemistry into a three-dimensional Lagrangian–Eulerian hybrid model: application to regional tropospheric ozone. Atmospheric Environment 34, 4361–4372.

Vitali, L., Monforti, F., Bellasio, R., Bianconi, R., Sachero, V., Mosca, S., Zanini, G., 2006. Validation of a Lagrangian dispersion model implementing different kernel methods for density reconstruction. Atmospheric Environment, in press, doi:10.1016/j.atmosenv.2006.06.056.

Zanini, G., Bellasio, R., Bianconi, R., Delle Monache, L., Kolarova, M., Lorenzini, R., Mosca, S., Monforti, F., Peverieri, S., Vitali, L., 2002. PLPM (Photochemical Lagrangian Particle Model): formulation and preliminary validation. In: Proceedings of Eighth International Conference on Harmonization within Atmospheric Dispersion Modelling for Regulatory Purposes, Sofia, October 2002.

Zanini, G., Monforti, F., Ornelli, P., Pignatelli, T., Vialetto, G., Brusasca, G., Calori, G., Finardi, S., Radice, P., Silibello, C., 2004. The MINNI Project. In: Proceedings of the Ninth International Conference on Harmonisation within Atmospheric Dispersion Modelling for Regulatory Purposes, Garmisch-Partenkirchen, June 2004.